Spin-polarized neutron matter: Critical unpairing and BCS-BEC precursor

Martin Stein* and Armen Sedrakian†
Institute for Theoretical Physics, J. W. Goethe-University, D-60438 Frankfurt am Main, Germany

Xu-Guang Huang‡
Physics Department & Center for Particle Physics and Field Theory, Fudan University, Shanghai 200433, China

John W. Clark§
Department of Physics and McDonnell Center for the Space Sciences, Washington University, St. Louis, Missouri 63130, USA and Centro de Ciências Matemáticas, University of Madeira, 9000-390 Funchal, Portugal

(Dated: January 26, 2016)

We obtain the critical magnetic field required for complete destruction of S-wave pairing in neutron matter, thereby setting limits on the pairing and superfluidity of neutrons in the crust and outer core of magnetars. We find that for fields $B \geq 10^{17}$ G the neutron fluid is non-superfluid – if weaker spin-1 superfluidity does not intervene – a result with profound consequences for the thermal, rotational, and oscillatory behavior of magnetars. Because the dineutron is not bound in vacuum, cold dilute neutron matter cannot exhibit a proper BCS-BEC crossover. Nevertheless, owing to the strongly resonant behavior of the nn interaction at low densities, neutron matter shows a precursor of the BEC state, as manifested in Cooper-pair correlation lengths being comparable to the interparticle distance. We make a systematic quantitative study of this type of BCS-BEC crossover in the presence of neutron fluid spin-polarization induced by an ultra-strong magnetic field. We evaluate the Cooper pair wave-function, quasiparticle occupation numbers, and quasiparticle spectra for densities and temperatures spanning the BCS-BEC crossover region. The phase diagram of spin-polarized neutron matter is constructed and explored at different polarizations.

PACS numbers: 21.65.+f, 21.30.Fe, 26.60.+c

arXiv:1510.06000v2 [nucl-th] 23 Jan 2016

I. INTRODUCTION

A comprehensive understanding of the thermodynamic properties of strongly magnetized baryonic matter is one of the major challenges in the astrophysics of compact stars. There is substantial observational evidence that anomalous x-ray pulsars and soft-γ-ray repeaters are two manifestations of strongly magnetized neutron stars, known as magnetars, which are characterized by surface fields of order $B \sim 10^{15}$ G [1]. These identifications are consistent with the measured slow spins and large spin-down rates as well as with the energetics of observed magnetic activity associated with flares. Magnetic fields play a secondary role in the structure and thermal emission of ordinary neutron stars with fields $B \sim 10^{12}$ G, whereas the fields in magnetars are large enough to impact basic physical properties of the stellar matter, including its equation of state, its crust composition, and its pairing and superfluid properties.

In this work we focus on the behavior of pure neutron matter in strong magnetic fields. Specifically, we have carried out a detailed study of S-wave pairing in neutron matter as it exits at relatively low densities. Our results are of two-fold interest. Firstly, we compute the critical magnetic field for unpairing of the S-wave condensate owing to the spin-alignment induced by the strong magnetic field, as measured by the spin polarization. The results are of direct practical interest for the astrophysics of magnetars, as the derived critical field for pair disruption limits the occurence of neutron superfluidity in the low-density (outer core and crust) regions of a neutron star. Second, we study the signatures of a BCS-BEC crossover [2] in dilute neutron matter and the emergence of dineutron correlations in a magnetic field, thus generalizing to the case of spin-polarized neutron matter the previous studies of this clustering phenomenon in infinite neutron matter [3–7] and in finite nuclear systems [8].

The BCS-BEC crossover, in the sense of Nozières-Schmitt-Rink theory [2], occurs naturally in the $^3S_1$-$^3D_1$ channel in isospin-symmetric [9–13] and isospin-asymmetric [14–16] nuclear matter, where the bound pairs are deuterons in the low-density limit. Neutron-neutron (nn) pairing in the $^1S_0$ channel comes into play in nuclear matter when the isospin asymmetry of the system is large enough to suppress the (otherwise dominant) attractive interaction the $^3S_1$-$^3D_1$ pairing channel. In pure neutron matter, isospin-triplet pairing in the $^3S_1$-$^3D_1$ channel is prohibited by Pauli blocking; hence the dominant pairing channel must be an isospin-singlet state, necessarily $^1S_0$ in the low-density regime, as implied by the nuclear phase-shift analysis (see Ref. [17]).

*Electronic address: mstein@th.physik.uni-frankfurt.de
†Electronic address: sedrakian@th.physik.uni-frankfurt.de
‡Electronic address: huangxuguang@fudan.edu.cn
§Electronic address: jwc@wuphys.wustl.edu

The primary effect of a magnetic field on a neutron Cooper pair is the alignment of their spins caused by the Pauli paramagnetic interaction between B field and the spin magnetic moments of the neutrons. Plainly, a large enough magnetic field will quench pairing. This nn pair-breaking effect may be contrasted with that for proton pairs (and ultimately charged hyperons), which become unpaired at lower field strengths owing to Landau diamagnetic currents [18–20].

The present description is constrained to the low-density regime below the saturation density of symmetrical nuclear matter, $\rho_0 = 0.16$ fm^{-3}. At higher densities the dominant pairing state in neutron matter shifts to the ${}^3P_2$-${}^3F_2$ channel, which induces a spin 1 condensate of neutrons [17]. In this case, the spin-polarizing effect of the magnetic field on the internal structure of the spin-1 pairs is nondestructive.

The two-neutron system has no bound state in vacuum, so dilution of neutron matter does not lead automatically to a state populated by tightly bound dineutrons that could undergo Bose-Einstein condensation (BEC). (It should be noted, however, that the bare neutron-neutron interaction in the ${}^1S_0$ channel supports a virtual state close to zero energy, which is characterized by a large scattering length -18.5 ± 0.4 fm. It thus implies a strongly correlated ${}^1S_0$-wave state at asymptotically low densities). Nevertheless, on general grounds one cannot expect a Bose condensate regime of neutrons to be present in the low-density limit. This situation stands in contrast to that for ${}^3S_1$-${}^3D_1$ neutron-proton (np) pairing, where the phase diagram exhibits both a BCS-BEC crossover region and a well-defined Bose condensate of deuterons at asymptotically low density. Notwithstanding the arguments above, it was shown in Refs. [3–6] that a BCS-BEC *crossover region* may also arise in neutron matter under dilution. In principle, this phenomenon occurs in full analogy to its counterpart for ${}^3S_1$-${}^3D_1$ pairing, with the exception that the asymptotical state of the system at low densities is a weakly interacting neutron gas, instead of a Bose condensate of neutron dimers.

The phase diagram of dilute neutron matter may contain anisotropic or non-homogeneous phases such as the Larkin-Ovchinnikov-Fulde-Ferrell (hereafter LOFF) phase or a phase-separated phase (see Refs. [15, 16] and references therein). Below we provide a theoretical framework which incorporates such phases; however, our numerical studies are confined to homogeneous, isotropic solutions.

Neutron-neutron pairing plays a prominent role in the physics of the inner crust of a neutron star (Ref. [17] and references therein). Other systems characterized by strong neutron excess are neutron-rich nuclei near the drip line [21–23] and halo nuclei such as ^{11}Li [24] that feature halo neutrons. There are conspicuous phenomenological signatures of neutron superfluidity in neutron stars, providing strong evidence that a neutron pairing condensate in the star's inner crust plays a prominent role in neutrino cooling and in glitch-type timing behavior in pulsars [17].

This paper is structured as follows. In Sec. II we give a brief presentation of the theory of spin-polarized neutron matter in terms of imaginary-time finite-temperature Green's functions. In Sec. III we discuss the results of extensive calculations based on this microscopic many-body approach, namely the phase diagram of neutron matter over the relevant low-density domain at various degrees of polarization, the temperature-polarization dependence of the gap in the weak-coupling regime, the kernel of the gap equation in various coupling regimes, the Cooper-pair wave function across the BCS-BEC crossover, and quasiparticle occupation numbers and dispersion relations. Section IV is concerned with the critical magnetic field required for unpairing of the condensate in the context of magnetars. Readers interested only in astrophysical implications of this work can skip directly to this section. Our conclusions are summarized in Sec. V.

II. THEORY

The theory of spin-polarized pair-correlated neutron matter in equilibrium can be formulated in the language of the imaginary-time Nambu-Gorkov matrix Green's function

$$i\mathscr{G}_{12} = i \begin{pmatrix} G^+_{12} & F^-_{12} \\ F^+_{12} & G^-_{12} \end{pmatrix} = \begin{pmatrix} \langle T_\tau \psi_1 \psi_2^+ \rangle & \langle T_\tau \psi_1 \psi_2 \rangle \\ \langle T_\tau \psi_1^+ \psi_2^+ \rangle & \langle T_\tau \psi_1^+ \psi_2 \rangle \end{pmatrix}, \quad (1)$$

where the indices $1, 2, \ldots$ stand for the continuous space-time variables $x = (t, \boldsymbol{r})$ of the neutrons, thus $G^+_{12} \equiv G^+_{\alpha\beta}(x_1, x_2)$, etc., and greek indices label discrete variables in general. In spin-polarized neutron matter the isospin is fixed, so within the discrete nucleonic degrees of freedom only the Pauli spins play a dynamical role. Therefore, each operator in Eq. (1) is a spinor, e.g., $\psi_\alpha = (\psi_{n\uparrow}, \psi_{n\downarrow})^T$, where the internal variables $\uparrow, \downarrow$ denote a particle's spin state. Accordingly, the propagators live in a 4×4 space owing to the doubling of degrees of freedom in the Nambu-Gorkov formalism and owing to the breaking of the spin $SU(2)$ symmetry.

The matrix propagator (1) obeys the standard Dyson equation, which we write in momentum space as

$$\left[\mathscr{G}_0(k, \boldsymbol{Q})^{-1} - \Xi(k, \boldsymbol{Q})\right] \mathscr{G}(k, \boldsymbol{Q}) = \mathbf{1}_{4\times 4}, \quad (2)$$

where $\Xi(k, \boldsymbol{Q})$ is the matrix self-energy. To accommodate in our formalism the appearance of the LOFF phase, we do not assume translational invariance from the outset. Hence the Green's functions and self-energies are allowed to depend on the center-of-mass momentum $\boldsymbol{Q}$ of Cooper pairs. The relative (four-)momentum of pairs is of the form $k \equiv (ik_\nu, \boldsymbol{k})$, in which the zeroth component assumes discrete values $k_\nu = (2\nu + 1)\pi T$, where $\nu \in \mathbb{Z}$ and T is the temperature. Further reductions are possible by virtue of the fact that the normal propagators for the particles and holes are diagonal in the spin space, the off-diagonal elements of the free matrix propagator $\mathscr{G}_0^{-1}$

being zero. Writing out the non-vanishing components in the Nambu-Gorkov space explicitly, we obtain

$$\mathscr{G}_0^{-1} = \begin{pmatrix} ik_\nu - \epsilon_\uparrow^+ & 0 & 0 & 0 \\ 0 & ik_\nu - \epsilon_\downarrow^+ & 0 & 0 \\ 0 & 0 & ik_\nu + \epsilon_\uparrow^- & 0 \\ 0 & 0 & 0 & ik_\nu + \epsilon_\downarrow^- \end{pmatrix}, \tag{3}$$

where

$$\epsilon_{\uparrow/\downarrow}^{\pm} = \frac{1}{2m^*}\left(\boldsymbol{k} \pm \frac{\boldsymbol{Q}}{2}\right)^2 - \mu_{\uparrow/\downarrow}. \tag{4}$$

These single-particle energies can be separated into symmetrical and anti-symmetrical parts with respect to time-reversal operation by writing

$$\epsilon_\uparrow^{\pm} = E_S - \delta\mu \pm E_A, \tag{5}$$
$$\epsilon_\downarrow^{\pm} = E_S + \delta\mu \pm E_A, \tag{6}$$

where

$$E_S = \frac{Q^2/4 + k^2}{2m^*} - \bar{\mu}, \tag{7}$$
$$E_A = \frac{\boldsymbol{k}\cdot\boldsymbol{Q}}{2m^*}, \tag{8}$$

are respectively the spin-symmetrical and spin-antisymmetrical parts of the quasiparticle spectrum and $\delta\mu \equiv (\mu_\uparrow - \mu_\downarrow)/2$ determines the shifts of chemical potentials of up-spin and down-spin neutrons from the mean $\bar{\mu} \equiv (\mu_\uparrow + \mu_\downarrow)/2$. The effective mass m^* is computed from a Skyrme density functional, with SkIII [25] and SLy4 [26] parametrizations yielding nearly identical results. The quasiparticle spectra in Eq. (3) are written in a general reference frame moving with the center-of-mass momentum $\boldsymbol{Q}$ relative to a laboratory frame at rest. The spectrum of quasiparticles is seen to be two-fold split owing to finite $\boldsymbol{Q}$ and further split owing to spin polarization, which breaks the spin $SU(2)$ internal symmetry of neutron matter.

As already stressed in the Introduction, low-density neutron matter interacts attractively in the $^1S_0$ channel, leading to isovector nn spin-singlet pairing. Accordingly, the anomalous propagators have the property $(F_{12}^+, F_{12}^-) \propto i\sigma_y$, where σ_y is the second Pauli matrix in spin space. This implies that in the quasiparticle approximation, the self-energy Ξ has only off-diagonal elements in Nambu-Gorkov space. The inverse full Green's function on the left-hand-side of Eq. (2) is then given by

$$\mathscr{G}^{-1} = \mathscr{G}_0^{-1} - \Xi = \begin{pmatrix} ik_\nu - \epsilon_\uparrow^+ & 0 & 0 & i\Delta \\ 0 & ik_\nu - \epsilon_\downarrow^+ & -i\Delta & 0 \\ 0 & i\Delta & ik_\nu + \epsilon_\uparrow^- & 0 \\ -i\Delta & 0 & 0 & ik_\nu + \epsilon_\downarrow^- \end{pmatrix}. \tag{9}$$

Thus, the Dyson equation takes the form

$$\begin{pmatrix} ik_\nu - \epsilon_\uparrow^+ & 0 & 0 & i\Delta \\ 0 & ik_\nu - \epsilon_\downarrow^+ & -i\Delta & 0 \\ 0 & i\Delta & ik_\nu + \epsilon_\uparrow^- & 0 \\ -i\Delta & 0 & 0 & ik_\nu + \epsilon_\downarrow^- \end{pmatrix} \cdot \begin{pmatrix} G_\uparrow^+ & 0 & 0 & F_{\uparrow\downarrow}^- \\ 0 & G_\downarrow^+ & F_{\downarrow\uparrow}^- & 0 \\ 0 & F_{\uparrow\downarrow}^+ & G_\uparrow^- & 0 \\ F_{\downarrow\uparrow}^+ & 0 & 0 & G_\downarrow^- \end{pmatrix} = \mathrm{diag}(1,1,1,1), \tag{10}$$

where we use short-hand $G_\uparrow^+ \equiv G_{\uparrow\uparrow}^+$ and so on. The solutions of this equation provide the normal and anomalous Green's functions

$$G_{\uparrow/\downarrow}^{\pm} = \frac{ik_\nu \pm \epsilon_{\downarrow/\uparrow}^{\mp}}{(ik_\nu - E_{\mp/\pm}^+)(ik_\nu + E_{\pm/\mp}^-)}, \tag{11}$$
$$F_{\uparrow\downarrow}^{\pm} = \frac{-i\Delta}{(ik_\nu - E_\pm^+)(ik_\nu + E_\mp^-)}, \tag{12}$$
$$F_{\downarrow\uparrow}^{\pm} = \frac{i\Delta}{(ik_\nu - E_\mp^+)(ik_\nu + E_\pm^-)}, \tag{13}$$

where the four branches of the quasiparticle spectrum are given by

$$E_r^a = \sqrt{E_S^2 + \Delta^2} + r\delta\mu + aE_A, \tag{14}$$

in which $a, r \in \{+,-\}$. In mean-field approximation, the anomalous self-energy (pairing-gap) is determined by

$$\begin{aligned}\Delta(\boldsymbol{k},\boldsymbol{Q}) = \frac{T}{4}\int\frac{d^3k'}{(2\pi)^3}\sum_\nu V(\boldsymbol{k},\boldsymbol{k}') \\ \times\mathrm{Im}[F_{\uparrow\downarrow}^+(k'_\nu,\boldsymbol{k}',\boldsymbol{Q}) + F_{\uparrow\downarrow}^-(k'_\nu,\boldsymbol{k}',\boldsymbol{Q}) \\ -F_{\downarrow\uparrow}^+(k'_\nu,\boldsymbol{k}',\boldsymbol{Q}) - F_{\downarrow\uparrow}^-(k'_\nu,\boldsymbol{k}',\boldsymbol{Q})],\end{aligned} \tag{15}$$

where $V(\boldsymbol{k},\boldsymbol{k}')$ is the neutron-neutron interaction potential. After partial-wave expansion in the potential we keep the ${}^1S_0$ component, compute the Matsubara sum and continue analytically to the real axis; as a result we find the gap equation

$$\Delta(Q) = \frac{1}{4}\sum_{a,r}\int \frac{d^3k'}{(2\pi)^3}V(k,k') \times \frac{\Delta(k',Q)}{2\sqrt{E_S^2(k')+\Delta^2(k',Q)}}[1-2f(E_r^a)], \quad (16)$$

where $f(E)$ is the Fermi function. The densities of up-spin and down-spin particles are given by

$$\rho_{\uparrow/\downarrow}(\boldsymbol{Q}) = T\int \frac{d^3k}{(2\pi)^3}\sum_\nu G^+_{\uparrow/\downarrow}(k_\nu,\boldsymbol{k},\boldsymbol{Q}). \quad (17)$$

Performing the same operations as for the gap function, we obtain

$$\rho_{\uparrow/\downarrow}(Q) = \int \frac{d^3k}{(2\pi)^3}\left[\frac{1}{2}\left(1+\frac{E_S}{\sqrt{E_S^2+\Delta^2}}\right)f(E^+_\mp) + \frac{1}{2}\left(1-\frac{E_S}{\sqrt{E_S^2+\Delta^2}}\right)(1-f(E^-_\pm))\right]. \quad (18)$$

At finite temperature T, the system minimizes its free energy by choosing the optimal values of the magnitude Q of the center-of-mass momentum and the gap in Eqs. (16) and (18). As a reference free energy we use the same quantity evaluated in the normal state with Q and Δ both zero, labeling it with an N subscript as opposed to the S subscript used for the superfluid state. Thus,

$$\mathcal{F}_S = \mathcal{E}_S - T\mathcal{S}_S \quad \text{versus} \quad \mathcal{F}_N = \mathcal{E}_N - T\mathcal{S}_N, \quad (19)$$

where $\mathcal{E}$ denotes the internal energy (statistical average of the system Hamiltonian) and $\mathcal{S}$ the entropy.

We measure the spin polarization by the parameter

$$\alpha = \frac{\rho_\uparrow - \rho_\downarrow}{\rho_\uparrow + \rho_\downarrow}, \quad (20)$$

where $\rho_\uparrow$ and $\rho_\downarrow$ are, respectively, the number densities of the up-spin and down-spin components of the neutron-matter system and $\rho = \rho_\uparrow + \rho_\downarrow$ is its total particle (or baryon) density. The possible solutions, or phases, of the variational problem so defined can be classified according to the alternatives

$$\begin{array}{lll} Q=0,\ \Delta\neq 0,\ x=0, & & \text{BCS phase,} \\ Q=0,\ \Delta=0,\ x=1, & & \text{unpaired phase,} \\ Q\neq 0,\ \Delta\neq 0,\ x=0, & & \text{LOFF phase,} \\ Q=0,\ \Delta\neq 0,\ 0<x<1, & & \text{phase-separated phase.} \end{array} \quad (21)$$

The ground state corresponds to the phase with lowest free energy. Below we will consider exclusively homogeneous, isotropic solutions corresponding, respectively, to the first two lines in Eq. (21); i.e., the anisotropic or inhomogeneous phases (the LOFF phase and the phase-separated phase) is not considered.

III. BCS PHASE, SEARCH FOR LOFF PHASE, AND CROSSOVER TO BEC

Based on calculations performed within the theoretical framework summarized in Sec. II, we have generated the temperature-density ($T-\rho$) phase diagram of dilute neutron matter at various spin polarizations [Eq. (20)]. A number of key quantities of the neutron condensate were studied at fixed T and ρ corresponding to the different coupling strengths which characterize the BCS versus quasi-BEC nature of the condensate. Table I collects several quantities of interest at fixed $T = 0.25$ MeV and vanishing spin polarization α, for three values of the density ρ that span the regimes studied numerically. The computations were carried out for the rank 3 separable Paris potential (PEST 3) in the ${}^1S_0$ partial-wave channel, with parameters given in Ref. [27].

Our findings concerning the BCS-BEC crossover are the following. No change of sign of the chemical potential was observed. The chemical potential $\bar{\mu}$ remains positive down to the lowest density considered. Specifically, the lowest value found for $\bar{\mu}$, 0.24 MeV, was obtained at the point $\ln(\rho/\rho_0) = -3.57$ and $T = 0.05$ where Δ vanishes within the numerical accuracy of our model. Our calculations indicate that the chemical potential vanishes asymptotically as the density tends to zero, without changing its sign. The absence of clear evidence of a BEC of dineutrons is the consequence of the fact that their mutual interaction in free space does not support a bound state. In other words, the free-space Schrödinger equation for neutrons does not have eigenvalues that correspond to a dineutron bound state. Even so, it should be acknowledged that we do find that the ratio of inter-neutron distance d and the condensate coherence length ξ_a satisfies the conditions $d/\xi_a \ll 1$ at high density (in the range under consideration) and $d/\xi_a \geq 1$ at low densities, consistent with the initial studies [3, 4]. The values of interparticle spacing d and coherence length ξ_a are shown for our model in Table I for the case of low temperature ($T = 0.25$ MeV) and vanishing spin polarization at three values of the density covering the low, intermediate, and high density regimes. It is seen that $d/\xi_a \sim 1$ at low densities, which is a clear sign of a BEC precursor. We address the effects of polarization on the BCS-quasi-BEC crossover in the following sections.

A. Phase diagram

The phase diagram was computed by solving Eqs. (16) and (18) self-consistently for the input pairing interaction in the ${}^1S_0$ channel. After the solutions were found we evaluated the free-energy (19) and found its minimum. The resulting phase diagram of neutron matter is shown in Fig. 1. Broadly speaking, we obtain the same structure as in the case of nuclear matter (cf. Fig. 1 of Ref. [15]). At low densities the critical temperature increases with increasing density, because the increase in the density of

$\log_{10}(\rho/\rho_0)$	k_F [fm^{-1}]	Δ [MeV]	m^*/m	μ_n [MeV]	d [fm]	$\xi_{\rm rms}$ [fm]	ξ_a [fm]
−1.0	0.78	2.46	0.967	12.94	2.46	4.87	4.33
−1.5	0.53	1.91	0.989	5.65	3.61	3.55	3.71
−2.0	0.36	1.07	0.997	2.49	5.30	2.36	4.48

TABLE I: (Color online) Tabulated values of characteristic parameters related to the $^1S_0$ condensate in dilute, unpolarized neutron matter at temperature $T = 0.25$ MeV, for selected values of the total particle density ρ (in units of the nuclear saturation density). Other table entries: Fermi momentum $k_F = (3\pi^2\rho)^{1/3}$, pairing gap Δ, effective mass (in units of bare mass), chemical potential μ_n, interparticle distance d, and coherence lengths $\xi_{\rm rms}$ and ξ_a.

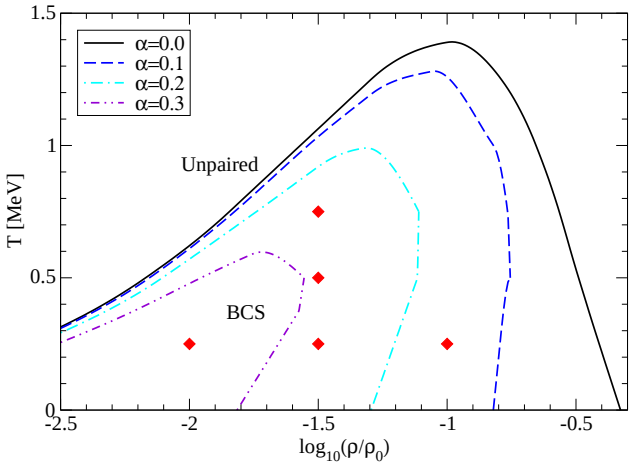

FIG. 1: (Color online) Phase diagram of neutron matter in the temperature-density plane for several spin polarizations α induced by magnetic fields. The BCS phase is naturally favored over the unpaired phase at lower temperatures and smaller polarizations. The red diamonds locate different points in the phase diagram at which some intrinsic features of low-density neutron matter have been evaluated.

states of neutrons compensates for the decrease in the attractive interaction strength in the S-wave channel with the increasing Fermi energy of the neutrons. This trend reverses at higher densities, and the pairing ceases at the point where the interaction in the $^1S_0$ channel becomes repulsive. Spin polarization suppresses pairing more efficiently in the high-density sector, where large portions of the phase diagram are converted from the superfluid to the normal phase already at moderate spin polarizations.

An interesting feature revealed in Fig. 1 is that the transition line separating unpaired and BCS phases is not a single-valued function of density in the range of densities considered. This behavior is well understood. Consider for example the dot-dash (light blue) transition line in the phase diagram corresponding the fixed polarization $\alpha = 0.2$. At low temperatures and not too low density, pairing is precluded because the reduced thermal smearing of the Fermi surfaces of the major and minor spin components cannot provide sufficient phase-space overlap of the corresponding Fermi quasiparticle distributions. The system remains in the normal, unpaired phase. Increasing the temperature at fixed density and polarization asymmetry increases the smearing effect, thereby enhancing the overlap enough to restore the BCS phase. We anticipate that some form of the LOFF phase may fill in the low temperature "pocket" formed by the inward turn of the phase separation boundary (cf. Fig. 1 of Ref. [15]). Note, however, that the pairing interaction in neutron matter is weaker than in nuclear matter; therefore the stability of the LOFF phase is not guaranteed.

B. Intrinsic properties of the neutron condensate

We now proceed to examine some intrinsic features of the isospin-triplet $^1S_0$ neutron condensate.

1. *Pairing gap*

In Figs. 2 and 3 we display the gap at fixed density $\log_{10}(\rho/\rho_0) = -1.5$. In Fig. 2 the gap is plotted as a function of temperature for several polarization values. For zero polarization, i.e., the case of the symmetrical BCS state, the value of the gap is maximal owing to perfect overlap of the Fermi surfaces of up-spin and down-spin particles. The temperature dependence of the gap corresponds to the standard BCS behaviour. Increasing the spin asymmetry has two effects. First, the gap is decreased owing to the separation of the Fermi surfaces, and so is the critical temperature T_c. Second, the maximum of the gap is shifted from $T = 0$ to nonvanishing temperatures. For large enough polarizations, this shift can lead to the appearance of a lower critical temperature.

Figure 3 shows the gap as a function of the polarization asymmetry parameter α over a range of temperatures. For $\alpha = 0$, increasing the temperature decreases the gap, as it should, according to BCS theory. The crossing of constant-temperature curves at finite α reflects the fact that raising the temperature from a relatively low value favors pairing in asymmetrical systems, by virtue of the increased overlap between the Fermi surfaces of the opposite-spin components. Of course, at high-enough

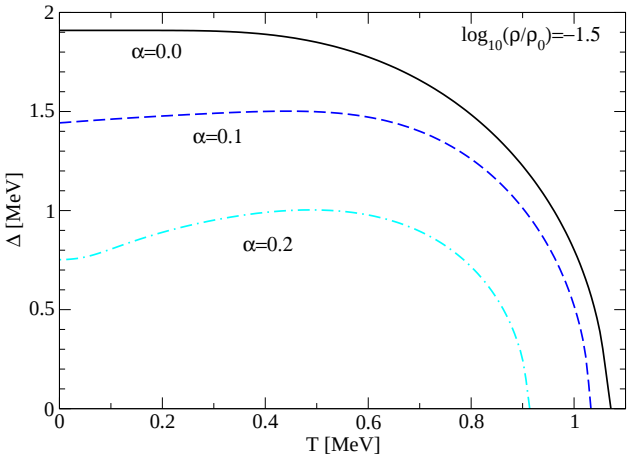

FIG. 2: (Color online) Pairing gap as a function of temperature at constant density index $\log_{10}(\rho/\rho_0) = -1.5$ for three choices of polarization parameter α.

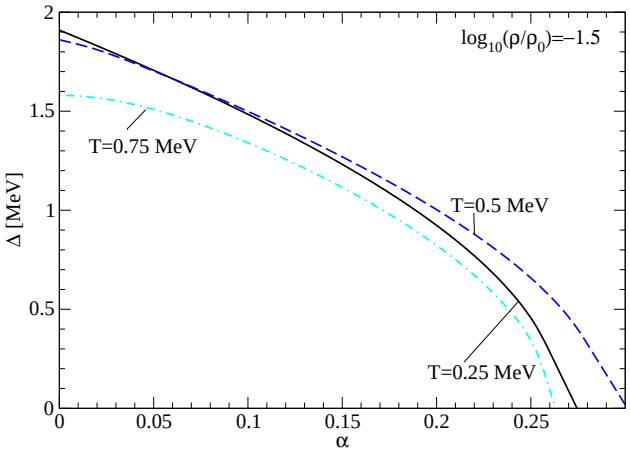

FIG. 3: (Color online) Pairing gap as a function of polarization at constant density index $\log_{10}(\rho/\rho_0) = -1.5$ for selected reference temperatures.

temperatures this effect must give way instead to the destruction of the superconducting state. These competing effects are reflected in the Fig. 3. At high-enough polarizations, the increase of temperature from $T = 0.25$ MeV to $T = 0.5$ MeV increases the gap, whereas the increase of temperature from $T = 0.5$ MeV to $T = 0.75$ MeV acts to reduce the gap. Note that allowing for the LOFF phase will modify the low-temperature behavior seen in Figs. 2 and 3 in a well-known manner [15, 16, 28].

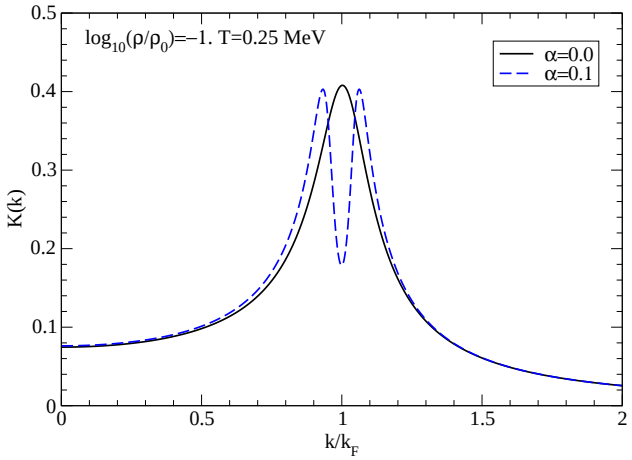

FIG. 4: (Color online) Dependence of the kernel $K(k)$ on momentum (in units of Fermi momentum) for fixed $\log_{10}(\rho/\rho_0) = -1$, $T = 0.25$ MeV, and polarization values color-coded in the inset.

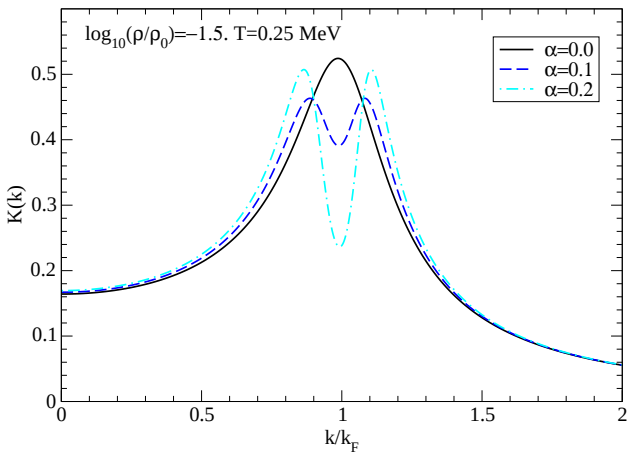

FIG. 5: (Color online) Same as Fig. 4, but for $\log_{10}(\rho/\rho_0) = -1.5$ and three polarization values color coded in the inset.

2. *Kernel of the gap equation*

In Figs. 4–7 we present the kernel of the gap equation for various values of density, temperature, and polarization in the BCS phase. The kernel of the gap equation is defined as

$$K(k) \;=\; \frac{1}{4}\sum_{a,r}\frac{1-2f(E_r^a)}{\sqrt{E_S^2(k)+\Delta^2(k)}}. \qquad (22)$$

Figures 4–6 show the kernel at $T = 0.25$ MeV for several values of the polarization, the density being fixed for each figure. As expected in the case of $\alpha = 0$ we find a single peak centered at the Fermi level. This peak

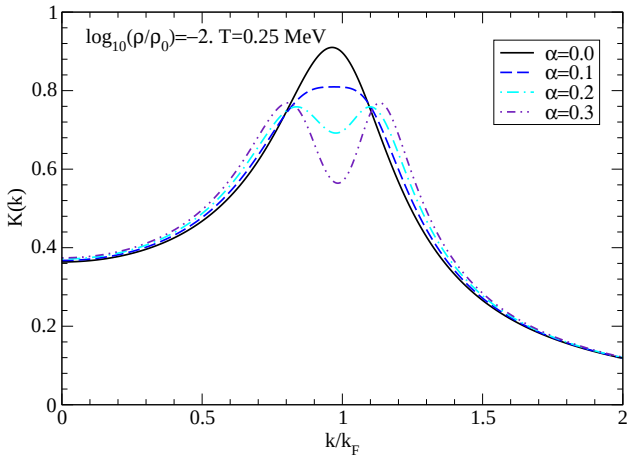

FIG. 6: (Color online) Same as Fig. 4 but for $\log_{10}(\rho/\rho_0) = -2$ and more polarization values.

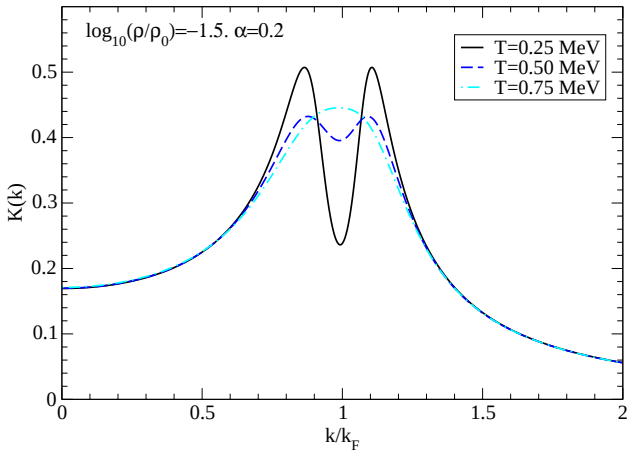

FIG. 7: (Color online) Dependence of the kernel $K(k)$ on momentum (in units of Fermi momentum) for fixed $\log_{10}(\rho/\rho_0) = -1$, $\alpha = 0.2$, and temperature values color coded in the inset.

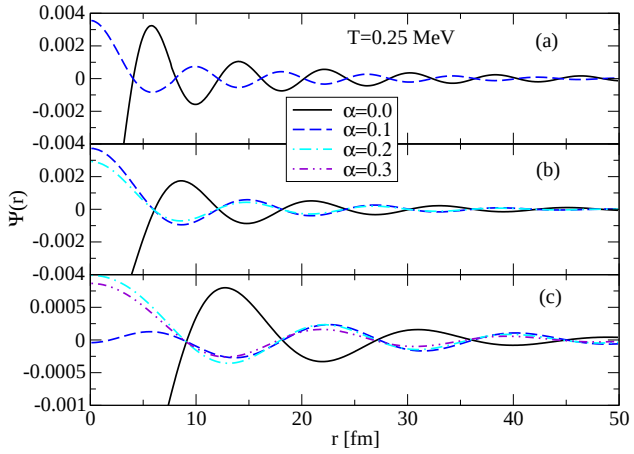

FIG. 8: (Color online) Plots of $\Psi(r)$ versus r at fixed temperature $T = 0.25$ MeV for three reference densities $\log_{10}(\rho/\rho_0) = -1$ (a), $\log_{10}(\rho/\rho_0) = -1.5$ (b), and $\log_{10}(\rho/\rho_0) = -2$ (c) and polarization values $\alpha = 0$ (solid line), 0.1 (dashed line), 0.2 (dash-dotted), and 0.3 (dashed-double-dotted).

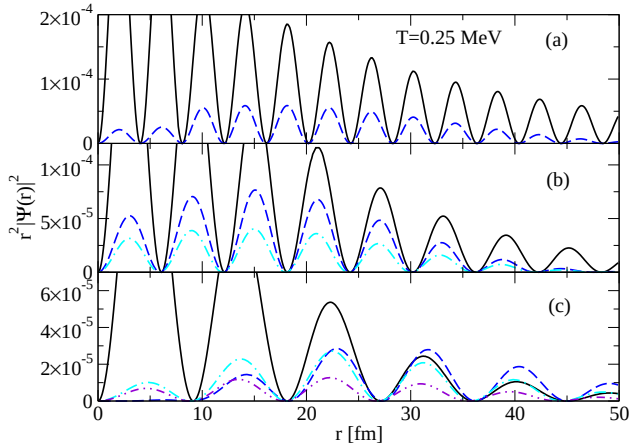

FIG. 9: (Color online) Same as Fig. 8, except $r^2|\Psi(r)|^2$ is plotted versus r.

separates into two for nonvanishing polarizations, simply reflecting the fact that there are now the two Fermi surfaces for up-spin and down-spin particles. In these figures one also observes that at high densities the peak of the kernel is located exactly at $k = k_F$, whereas for low densities the peak is shifted to momenta below the corresponding k_F. Additionally, at lower densities the polarization-induced two-peak structure is smeared; this is naturally attributed to the weakening of the degeneracy of the system.

The kernel evaluated at constant density and polarization is exhibited in Fig. 7 for three different temperatures. One clearly recognizes a thermal smearing of the polarization-induced two-peak structure, which evolves into a one-peak structure at high temperatures.

3. *Cooper-pair wave function*

Next we discuss the Cooper-pair wave function $\Psi(r)$ and the quantity $r^2|\Psi(r)|^2$, which determines the second moment of the density distribution of Cooper pairs. With the wave function at our disposal, we also have numerical access to the correlation length $\xi_{\rm rms}$ of the condensate, which can then be compared with the analytical BCS

expression for the coherence length ξ_a and with the interparticle distance d. The wave function is obtained by the Fourier transformation as

$$\Psi(r) \;=\; \frac{\sqrt{N}}{2\pi^2 r}\int_0^\infty dp\, p\,[K(p,\Delta)-K(p,0)]\sin(pr)\,, \tag{23}$$

with normalization satisfying

$$1 \;=\; N\int d^3r|\Psi(r)|^2. \tag{24}$$

The root-mean-square (rms) value for the coherence length is given by

$$\xi_{\rm rms} \;=\; \sqrt{\langle r^2\rangle}\,, \tag{25}$$

where

$$\langle r^2\rangle \;\equiv\; \int d^3r\, r^2|\Psi(r)|^2. \tag{26}$$

The analytical BCS result for the coherence length is given by

$$\xi_a \;=\; \frac{\hbar^2 k_F}{\pi m^*\Delta}\,, \tag{27}$$

where now Δ is the pairing gap in the $^1S_0$ channel and m^* is the effective mass of neutrons. Finally, the interparticle distance is simply related to the total particle density of the system by

$$d \;=\; \left(\frac{3}{4\pi\rho}\right)^{1/3}. \tag{28}$$

Table I displays the quantities defined above at vanishing polarization and fixed temperature $T = 0.25$ MeV. For each of three representative densities, corresponding values are entered for k_F, Δ, m^*/m, μ_n, d, $\xi_{\rm rms}$, and ξ_a. At high density it is seen that $\xi_{\rm rms} \simeq \xi_a$, i.e., the BCS analytical expression is a good approximation to the numerically computed coherence length. This is not the case at low densities, where one can only rely on the numerical value $\xi_{\rm rms}$ produced by our theoretical treatment. At any rate, comparison of the numerically generated coherence length with the interparticle distance shows a clear signature of a BCS-BEC crossover: For $\log_{10}(\rho/\rho_0) = -1$ we find $\xi_{\rm rms}/d \simeq 2$, whereas for $\log_{10}(\rho/\rho_0) = -2$ the pertinent ratio is $\xi_{\rm rms}/d \simeq 0.45$. Below we will trace, in other variables, further signatures of a BCS-BEC crossover in spin-polarized neutron matter.

In Fig. 8 the Cooper-pair wave function $\Psi(r)$ is plotted against radial distance at fixed temperature $T = 0.25$ MeV and various polarization values, for the three fiducial densities adopted in Table I. In all cases we find strongly oscillating wave functions. For nonvanishing polarization, the wave function experiences a sign change; the oscillations are then in counterphase to the unpolarized case. With increasing polarization, the amplitude of $\Psi(r)$ decreases in accord with the consequent reduction of the pairing gap. Furthermore, as the oscillation periods are given roughly by $2\pi/k_F$, a decrease of density and hence of Fermi momentum leads to an increase of oscillation period. The degree of polarization does not affect the period, which is determined by k_F values. Figure 9 shows $r^2|\Psi(r)|^2$ as a function of radial distance, the oscillatory behavior observed in Fig. 8 being reflected quite naturally in this quantity. However, two features are made more apparent in Fig. 9. At the lowest density considered, (i) the maxima of this wave function measure plotted for different polarizations are shifted with respect to each other and (ii) the overall maximum attained for each polarization is not situated at the same value of r (although this does become the case at higher densities).

4. *Quasiparticle occupation numbers*

In this section, we analyze the behavior of the occupation numbers of up-spin and down-spin neutrons in spin-polarized pure neutron matter. The occupation numbers are given by the integrand of Eq. (18). Explicitly,

$$\begin{aligned} n_{\uparrow/\downarrow}(k) \;&=\; \frac{1}{2}\left(1+\frac{E_S}{\sqrt{E_S^2+\Delta^2}}\right) f(E_\mp) \\ &+\; \frac{1}{2}\left(1-\frac{E_S}{\sqrt{E_S^2+\Delta^2}}\right)[1-f(E_\pm)]\,, \end{aligned} \tag{29}$$

with $E_r^a \to E_r$ for BCS pairing with $\boldsymbol{Q} = 0$, i.e., $E_A = 0$ in Eq. (8). It may be noted in passing that the functions $n_{\uparrow/\downarrow}(k)$ have maximum value 1, rather than the value 2 appropriate to nuclear matter (which reflects a summation over spin).

Figures 10–12 display the occupation numbers of up-spin and down-spin neutrons at fixed temperature $T = 0.25$ MeV and fixed densities $\log_{10}(\rho/\rho_0) = -1$, -1.5, and -2 respectively. The chosen polarization values are indicated in each figure. We observe that in the case of vanishing polarization (solid lines), the Fermi-step-like occupation present in the high-density limit has evolved into an increasingly flatter distribution at low densities, the Fermi surface growing ever more diffuse with decreasing density. At finite polarizations, the occupation numbers (or occupation probabilities) of up-spin and down-spin neutrons "split," or separate from one another, into distinct curves in the region around k_F. In fact, the locations of the drop-offs in the occupancies of these two spin populations agree well with their corresponding Fermi wave numbers. At high densities, the polarization-induced splitting results in a "breach" for large asymmetries with $n_{n\uparrow} \approx 1$ and $n_{n\downarrow} \approx 0$ around k_F. (The notion of breach and "breached pairing" in the same context was introduced for ultracold atoms in Ref. [29]). The breach remains intact at lower densities, but the slope of the corresponding occupation probabilities declines, as already remarked for the case of unpolarized matter.

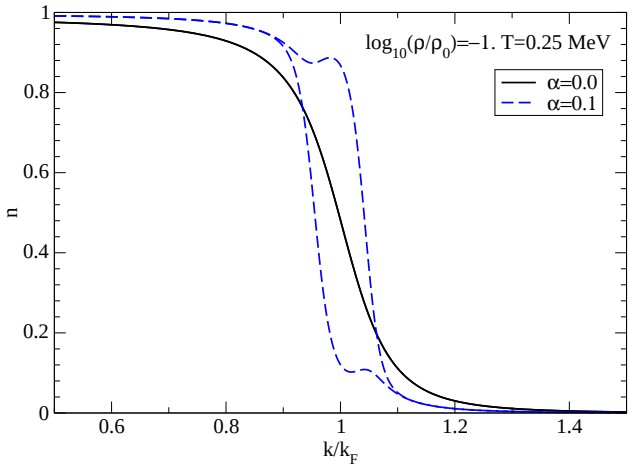

FIG. 10: (Color online) Dependence of the up-spin and down-spin neutron occupation numbers on momentum k (in units of Fermi momentum) for fixed $\log_{10}(\rho/\rho_0) = -1$, $T = 0.25$ MeV, and polarization values color coded in the inset.

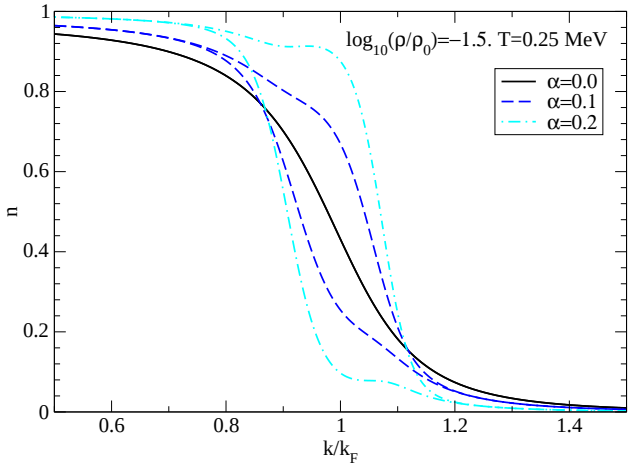

FIG. 11: (Color online) Same as Fig. 10, but for $\log_{10}(\rho/\rho_0) = -1.5$ and an additional polarization value.

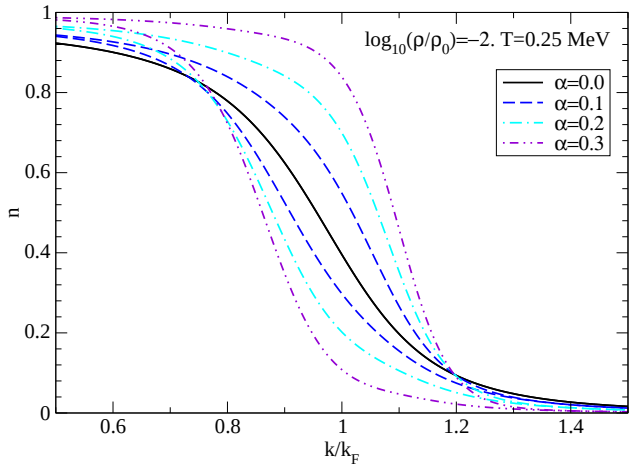

FIG. 12: (Color online) Same as Fig. 11, but for $\log_{10}(\rho/\rho_0) = -2$ and an additional polarization value.

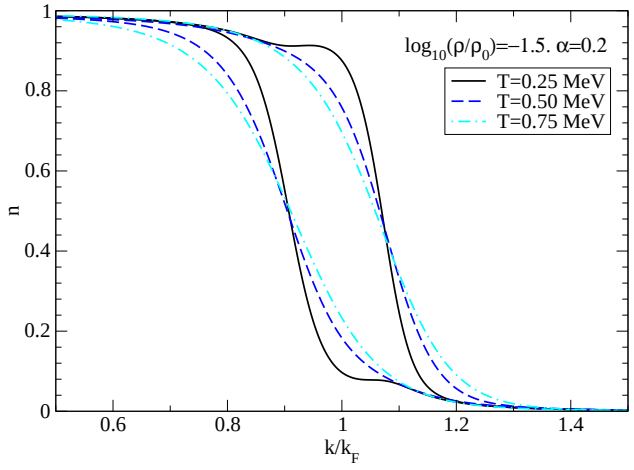

FIG. 13: (Color online) Dependence of the up-spin and down-spin neutron occupation numbers on momentum k (in units of Fermi momentum) for fixed $\log_{10}(\rho/\rho_0) = -1.5$, $\alpha = 0.2$, and temperatures color coded in the inset.

In Fig. 13 we show the occupation numbers of up-spin and down-spin neutrons at fixed density $\log_{10}(\rho/\rho_0) = -1.5$ and fixed polarization $\alpha = 0.2$ for different temperatures. As clearly seen, the occupation probabilities are subjected to greater smearing with increasing temperature.

5. *Quasiparticle spectra*

Turning to the final intrinsic property of interest, we examine the dispersion relations for quasiparticle excitations about the ${}^1S_0$ pairing condensate. Because a LOFF phase does not enter the picture here, the quasiparticle branches $E^-_\pm$ and $E^+_\pm$ coincide and the superscript may be dropped, leaving just two branches

$$E_\pm(k) \;=\; \sqrt{\left(\frac{k^2}{2m^*} - \bar{\mu}\right)^2 + \Delta^2} \pm \delta\mu. \qquad (30)$$

These dispersion relations are plotted in Fig. 14 for various values of density and polarization at fixed temperature $T = 0.25$ MeV. In each case the spectrum has a minimum at k_F. At finite polarization there is a splitting of the spectra of up-spin and down-spin neutrons.

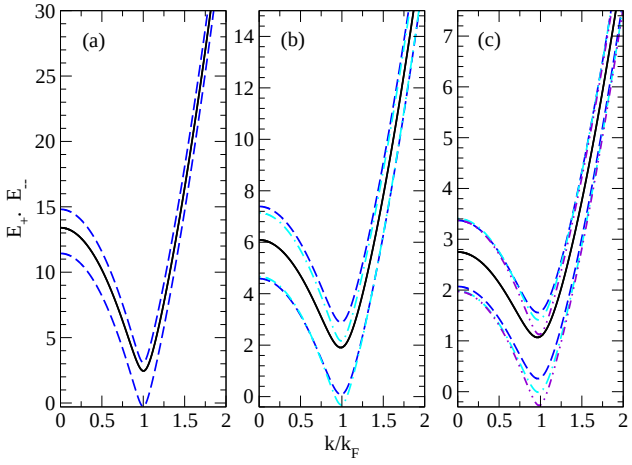

FIG. 14: (Color online) Dispersion relations for quasiparticle spectra in the BCS condensate, as functions of momentum (in units of Fermi momentum) for three densities $\log_{10}(\rho/\rho_0) = -1$ (a), $\log_{10}(\rho/\rho_0) = -1.5$ (b), and $\log_{10}(\rho/\rho_0) = -2$ (c). The polarization values are $\alpha = 0$ (solid line), 0.1 (dashed line), 0.2 (dash-dotted), 0.3 (dashed-double-dotted). For each polarization, the upper branch corresponds to the E_+ solution, the lower branch to the E_- solution.

A special feature that deserves notice is that at low densities the spectrum of the minority component (e.g., the down-spin neutrons) crosses zero, which implies that its spectrum is gapless.

IV. CRITICAL UNPAIRING IN NEUTRON MATTER

It is elementary that spin polarization in pure neutron matter can be induced by a magnetic field. A given polarization corresponds to shifts having equal magnitude $|\delta\mu|$ xof the chemical potentials $\mu_\uparrow$ and $\mu_\downarrow$ of the up-spin and down-spin components relative to their common chemical potential at zero polarization. The required field magnitude is then given by

$$|\delta\mu| = |\tilde{\mu}_N| B, \tag{31}$$

where

$$\tilde{\mu}_N = g_n \frac{m_n}{m_n^*} \mu_N \tag{32}$$

is the spin magnetic moment of the neutron, with $g_n = -1.91$ its g factor and m^* its effective mass, $\mu_N = e\hbar/2mc$ being the nuclear magneton (in cgs units). Thus, the magnetic field involved is linearly related to the shift of chemical potentials for a specified spin polarization.

In Fig. 15 we display results for the requisite magnetic field as a function of density at constant polarization and temperature. In the main, this figure tells us that a larger magnetic field is needed to obtain a given spin polarization as the density increases. In other words, dense neutron matter is harder to polarize than low-density neutron matter. However, this trend reverses at and above approximately one-tenth the saturation density ρ_0. The underlying physical content of this observation is difficult to access because the chemical potential shift is non trivially related to both the polarization (the density asymmetry of up-spin and down-spin components) and the pairing gap. It is further seen from Figure 15

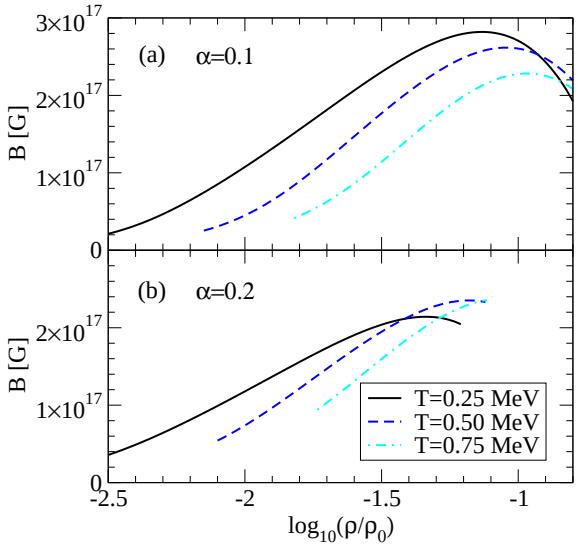

FIG. 15: (Color online) Magnetic field required to create a specified spin polarization as a function of the density for two polarization values $\alpha = 0.1$ (a) and 0.2 (b) and temperatures $T = 0.25$ (solid line), 0.5 (dashed line), and 0.75 (dash-dotted line).

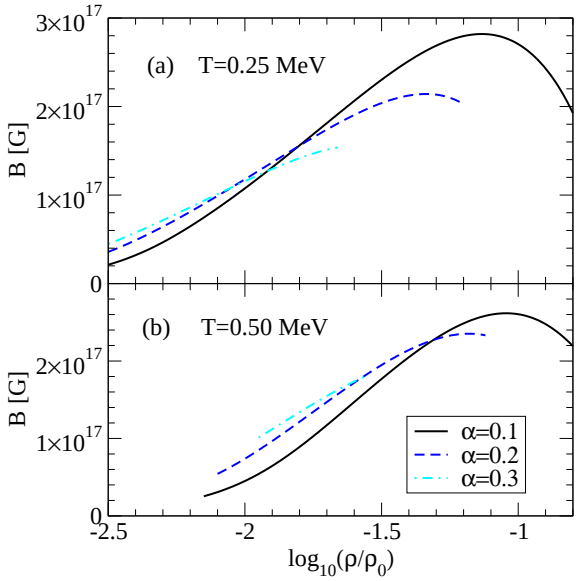

FIG. 16: (Color online) Same as Fig. 15 for two temperatures $T = 0.25$ MeV (a) and 0.5 MeV (b) and for several polarizations $\alpha = 0$ (solid line), 0.2 (dashed line), 0.3 (dash-dotted line).

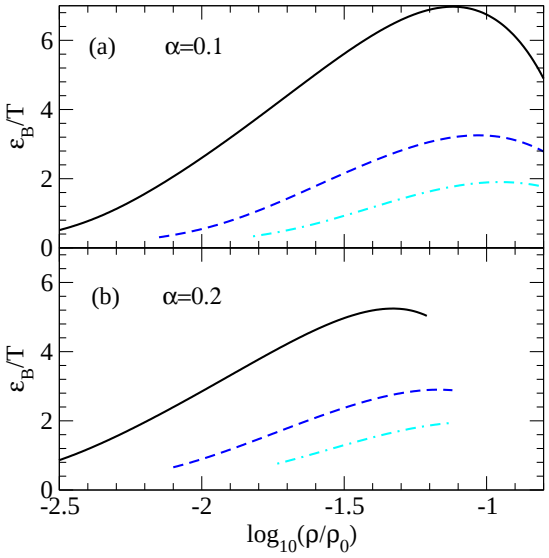

FIG. 17: (Color online) Ratio of magnetic energy to temperature as a function of density for two polarization values $\alpha = 0.1$ (a) and 0.2 (b) and temperatures $T = 0.25$ (solid line), 0.5 (dashed line), and 0.75 (dash-dotted line).

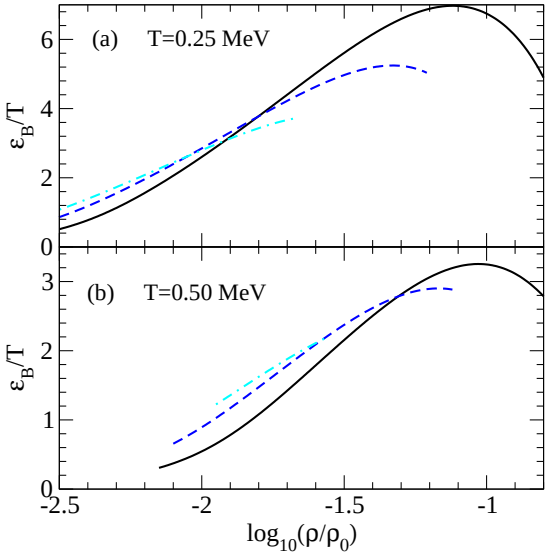

FIG. 18: (Color online) Ratio of magnetic energy to temperature as a function of density for two temperatures $T = 0.25$ MeV (a) and 0.5 MeV (b) and for several polarizations $\alpha = 0$ (solid line), 0.2 (dashed line), 0.3 (dash-dotted line).

that higher-temperature neutron matter is more easily polarizable at low densities, but this trend may again reverse at higher densities. Fig. 16 provides an alternative view of the same information, now with the temperature fixed in each panel and lines of fixed polarization color coded. From this view we infer that a larger magnetic field is needed to achieve a larger polarization in low-density neutron matter. However, this trend may again reverse at higher densities.

It is conceptually interesting to examine the ratio of

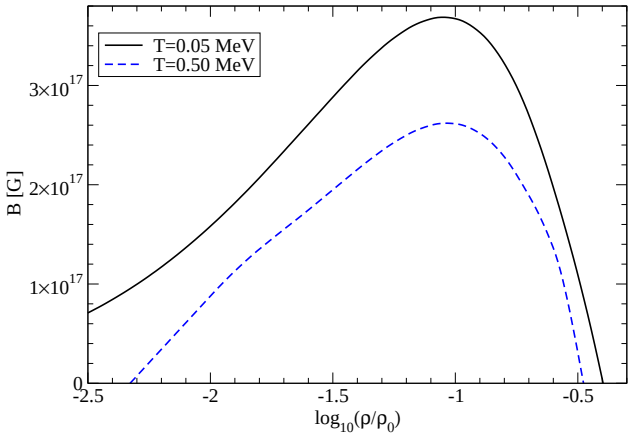

FIG. 19: (Color online) Unpairing magnetic field as a function of density (in units of ρ_0) for $T = 0.05$ (solid line) and $T = 0.5$ MeV (dashed line).

the magnetic energy (associated with the neutron spin's interaction with the magnetic field) to the temperature, i.e., the ratio

$$\frac{\varepsilon_B}{T} \simeq \frac{|\tilde{\mu}_N|B}{T}. \tag{33}$$

For degenerate neutrons the transport and radiation processes involve neutrons located in the narrow strip of width $\sim T$ around the Fermi surface; the magnetic field influences these processes when this ratio becomes of the order unity. It is shown in Figs. 17 and 18, where the arrangement of the panels and the color coding are analogous to those of Figs. 15 and 16, respectively. It is seen that $\epsilon_B/T \gg 1$ over almost the complete range of the parameter space, with exceptions only at very low densities. This implies that the dynamical processes in neutron fluid will be strongly affected by the field if the blocking effect of the pairing gap can be surmounted, e. g., when $\Delta(T, \alpha) \leq T$.

Finally, we consider the critical magnetic field that completely destroys the $^1S_0$ Cooper pairs in neutron matter by aligning the neutron spins in each pair. As a function of density, this field, shown in Fig. 19, has a shape that naturally reflects the corresponding density dependence of the pairing field. Accordingly, it is largest at $T \to 0$ and decreases as the pairing gap decreases with increasing temperature.

The strengths of the B fields in the crust and outer-core regions of magnetars are unknown, although it is anticipated that their interior fields could be much larger than the surface fields $B \sim 10^{15}$ G inferred from observations. A number of magnetar models entertain the possibility that strong toroidal B-fields are confined to the crust of the magnetar. If large enough ($B > B_{\rm cr}$), the magnetic field will locally eliminate neutron superfluidity. In particular, according to Fig. 19, the neutron fluid in magnetars will be non-superfluid (i.e., in a normal phase) for $B > 3 \times 10^{17}$ G. The non-superfluidity or partial

superfluidity of magnetars will clearly have profound implications for their neutrino emissivities, transport properties, and thermal evolution, as well such dynamical aspects as the damping of stellar oscillations and the interpretation of rotational anomalies such as glitches and anti-glitches. Note that the proton superconductivity in magnetar cores will be destroyed by Landau diamagnetic currents for fields even lower than those needed for the destruction of neutron S-wave superfluidity [19, 20]. Of course the Pauli paramagnetic destruction mechanism discussed here for S-wave paired neutrons will apply to S-wave paired protons as well, but the diamagnetic mechanism is more important for protons.

V. CONCLUSIONS

We have studied the phase diagram of dilute, spin-polarized neutron matter with a BCS type order parameter. Because two neutrons are unable to form a bound pair in free space, there exists no *a priori* case for the BEC of neutron-neutron pairs. However, the application of Nozières-Schmitt-Rink theory [2] led us to establishing a number of signatures in neutron matter that can be interpreted as a precursor of BCS-BEC crossover; in the limit of zero polarization these findings are in agreement with earlier studies of this phenomenon [3–7]. Our conclusion can be summarized as follows:

(i) At low density, spin polarization does not affect the pairing substantially, but for higher densities and high polarizations, the pairing gap and hence the critical temperature T_c are significantly suppressed. At finite polarization and low temperatures, we find a lower critical temperature that emerges from the combined effects of a polarization-induced separation and temperature-induced smearing of the Fermi surfaces involved. This feature tentatively indicates the possibility of the LOFF phase filling the low-temperature and high-density region of the phase diagram.

(ii) We have analyzed some intrinsic features of the spin-polarized neutron condensate, specifically the gap, the kernel of the gap equation, the pair-condensate wave function, and the quasiparticle occupation numbers and energy spectra. Similarities to behaviors found in a corresponding study of low-density isospin-asymmetric nuclear matter [15, 16] have been highlighted, along with their differences. We focus below on the principal findings of this analysis.

(iii) Under significant polarization, the kernel of the gap equation acquires a double-peak structure in momentum space, in contrast to the single peak present in the unpolarized case at the Fermi momentum k_F. This feature is most pronounced in the high-density and low-temperature limits. Decreasing the density (or increasing the temperature) smears out these structures.

(iv) The Cooper-pair wave functions exhibit oscillatory behavior. At finite polarization the oscillations are in counterphase to those of the unpolarized case. The period of the oscillations is set by the wave vector as $2\pi/k_F$ and is not affected by the polarization.

(v) The quasiparticle occupation numbers show a separation of the majority and minority spin populations by a breach around the Fermi momentum k_F. This is most pronounced in the high-density and low-temperature limit, with the minority-spin component becoming almost extinct. For high temperatures or low densities, this breach is smeared out.

(vi) Study of the quasiparticle dispersion relations establishes that they have a standard BCS form in the unpolarized case and split into two branches at finite polarization, while retaining the general BCS shape. These spectra have minima at $k = k_F$, as required. At large polarizations the energy spectrum of the minority-spin particles crosses the zero-energy level, which is a signature of gapless superconductivity. In other words, the Fermi surface of the minority particles features locations where modes can be excited without any energy cost.

(vii) At low densities, a relatively low magnetic field is sufficient to generate a given polarization. In general, the magnetic field required to produce a certain polarization increases with decreasing temperature and with increasing polarization.

(viii) Finally, we have determined the critical field for unpairing of the neutron condensate, which turns out to be in the range $B \sim 10^{17}$ G. For larger fields the neutron fluid is non superfluid, which would have profound consequences for the thermal, rotational and oscillatory behavior of magnetars.

Looking ahead, it should be mentioned that the present discussion does not take into account modifications of the pairing interaction in the medium, i.e., screening of the nuclear interaction. In the case of unpolarized neutron matter, screening effects have been discussed extensively; see Ref. [17] and references cited therein, and especially Refs. [4, 12] in the context of the BCS-BEC crossover. It is expected that pairing correlations are suppressed by the spin-fluctuation part of the screening interaction; hence the magnitude of the pairing gap and the range of densities over which pairing correlations extend will be reduced compared to what we find in the present study. This is strictly true if the spin-polarization does not change the sign of the screening interaction between neutrons. We anticipate that the changes will be of quantitative nature, without affecting the topology and the shape of the phase diagram of Fig. 1. Accordingly, the

main implication of the suppression of pairing by screening for the results we report is that the critical unpairing magnetic field obtained is an *upper bound*. A more complete application of our microscopic analysis to neutron star crusts would require the inclusion of nuclear clusters, as well as modifications of their properties induced by strong B fields [30]. At those densities where apart from leading S-wave interaction, a subdominant P-wave interaction exists, the suppression of the S-wave pairing may give rise to P-wave superfluid, rather than normal spin-polarized fluid.

Another relevant aspect of the many-body theory of this problem is that neutron matter is close to the unitary limit because of the large nn scattering length. Universal relations can be obtained in this limit, in particular for critical fields, with naive applications to neutron matter leading to estimates [31] consistent with those derived here.

Acknowledgments

M. S. acknowledges support from the HGS-HIRe graduate program at Frankfurt University. A. S. is supported by the Deutsche Forschungsgemeinschaft (Grant No. SE 1836/3-1) and by the NewCompStar COST Action MP1304. X. G. H. is supported by Fudan University Grant EZH1512519 and Shanghai Natural Science Foundation Grant No.14ZR1403000. J. W. C. acknowledges research support from the McDonnell Center for the Space Sciences and expresses his thanks to Professor José Luís da Silva and his colleagues at Centro de Ciências Matemáticas for gracious hospitality at the University of Madeira.

[1] C. Thompson and R. C. Duncan, MNRAS **275**, 255 (1995).
[2] P. Nozières and S. Schmitt-Rink, Journal of Low Temperature Physics **59**, 195 (1985).
[3] M. Matsuo, Phys. Rev. C **73**, 044309 (2006), nucl-th/0512021.
[4] J. Margueron, H. Sagawa, and K. Hagino, Phys. Rev. C **76**, 064316 (2007), 0710.4241.
[5] T. Abe and R. Seki, Phys. Rev. C **79**, 054003 (2009), 0708.2524.
[6] B. Y. Sun and W. Pan, Nuclear Physics A **909**, 8 (2013), 1304.6254.
[7] V. A. Khodel, J. W. Clark, V. R. Shaginyan, and M. V. Zverev, Physics of Atomic Nuclei **77**, 1145 (2014), 1310.5342.
[8] Y. Kanada-En'yo, N. Hinohara, T. Suhara, and P. Schuck, Phys. Rev. C **79**, 054305 (2009), 0902.3717.
[9] T. Alm, B. L. Friman, G. Röpke, and H. Schulz, Nuclear Physics A **551**, 45 (1993).
[10] M. Baldo, U. Lombardo, and P. Schuck, Phys. Rev. C **52**, 975 (1995).
[11] A. Sedrakian and J. W. Clark, Phys. Rev. C **73**, 035803 (2006), nucl-th/0511076.
[12] X.-G. Huang, Phys. Rev. C **81**, 034007 (2010), 1002.0060.
[13] T. T. Sun, B. Y. Sun, and J. Meng, Phys. Rev. C **86**, 014305 (2012), 1206.3407.
[14] U. Lombardo, P. Nozières, P. Schuck, H.-J. Schulze, and A. Sedrakian, Phys. Rev. C **64**, 064314 (2001), nucl-th/0109024.
[15] M. Stein, X.-G. Huang, A. Sedrakian, and J. W. Clark, Phys. Rev. C **86**, 062801 (2012), 1208.0123.
[16] M. Stein, A. Sedrakian, X.-G. Huang, and J. W. Clark, Phys. Rev. C **90**, 065804 (2014), 1410.1053.
[17] A. Sedrakian and J. W. Clark, *Nuclear Superconductivity in Compact Stars: BCS Theory and Beyond* (World Scientific Publishing Co, 2006), p. 135.
[18] N. W. Ashcroft and Mermin, *Introduction to Solid State Physics* (John Wiley & Sons, 2005).
[19] M. Sinha and A. Sedrakian, Phys. Rev. C **91**, 035805 (2015), 1502.02979.
[20] M. Sinha and A. Sedrakian, Physics of Particles and Nuclei **46**, 1510 (2015), 1403.2829.
[21] G. F. Bertsch and H. Esbensen, Annals of Physics **209**, 327 (1991).
[22] A. Pastore, J. Margueron, P. Schuck, and X. Viñas, Phys. Rev. C **88**, 034314 (2013), 1303.5651.
[23] Y. Zhang, M. Matsuo, and J. Meng, Phys. Rev. C **90**, 034313 (2014), 1310.3625.
[24] K. Hagino, H. Sagawa, and P. Schuck, Journal of Physics G Nuclear Physics **37**, 064040 (2010), 0912.4792.
[25] R. K. Su, S. D. Yang, and T. T. S. Kuo, Phys. Rev. C **35**, 1539 (1987).
[26] E. Chabanat, P. Bonche, P. Haensel, J. Meyer, and R. Schaeffer, Nuclear Physics A **635**, 231 (1998).
[27] J. Haidenbauer and W. Plessas, Phys. Rev. C **30**, 1822 (1984).
[28] L. He, M. Jin, and P. Zhuang, Phys. Rev. B **74**, 214516 (2006), cond-mat/0606322.
[29] E. Gubankova, W. V. Liu, and F. Wilczek, Physical Review Letters **91**, 032001 (2003), hep-ph/0304016.
[30] N. Chamel, R. L. Pavlov, L. M. Mihailov, C. J. Velchev, Z. K. Stoyanov, Y. D. Mutafchieva, M. D. Ivanovich, J. M. Pearson, and S. Goriely, Phys. Rev. C **86**, 055804 (2012), 1210.5874.
[31] L. He and P. Zhuang, Phys. Rev. B **83**, 174504 (2011), 1101.5694.